ARTICLE

Quantifying Resistances across Nanoscale Low- and High-Angle Interspherulite Boundaries in Solution-Processed Organic Semiconductor Thin Films

Stephanie S. Lee,[†] Jeffrey M. Mativetsky,[†] Marsha A. Loth,[‡] John E. Anthony,[‡] and Yueh-Lin Loo[†,*]

[†]Department of Chemical and Biological Engineering, Princeton University, Princeton, New Jersey 08544, United States and [‡]Department of Chemistry, University of Kentucky, Lexington, Kentucky 40506, United States

ABSTRACT The nanoscale boundaries formed when neighboring spherulites impinge in polycrystalline, solution-processed organic semiconductor thin films act as bottlenecks to charge transport, significantly reducing organic thin-film transistor mobility in devices comprising spherulitic thin films as the active layers. These interspherulite boundaries (ISBs) are structurally complex, with varying angles of molecular orientation mismatch along their lengths. We have successfully engineered exclusively low- and exclusively high-angle ISBs to elucidate how the angle of molecular orientation mismatch at ISBs affects their resistivities in triethylsilylethynyl anthradithiophene thin films. Conductive AFM and four-probe measurements reveal that current flow is unaffected by the presence of low-angle ISBs, whereas current flow is significantly disrupted across high-angle ISBs. In the latter case, we estimate the resistivity to be 22 M$\Omega\mu m^2$/width of the ISB, only less than a quarter of the resistivity measured across low-angle grain boundaries in thermally evaporated sexithiophene thin films. This discrepancy in resistivities across ISBs in solution-processed organic semiconductor thin films and grain boundaries in thermally evaporated organic semiconductor thin films likely arises from inherent differences in the nature of film formation in the respective systems.

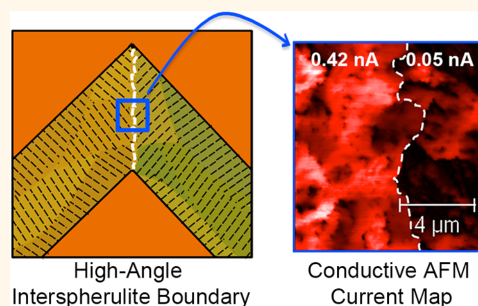

KEYWORDS: spherulite · interspherulite boundary · grain boundary · organic semiconductor · solution processing

Solution-processable organic semiconductors are promising candidates as active layers in organic thin-film transistors (OTFTs) for radio frequency identification tags and active matrix displays.[1] These compounds are compatible with high-throughput, large-area deposition methods, such as inkjet printing;[2] processing the active layers of devices from solution can thus dramatically lower the cost of electronics. With the advantage of rapid deposition, however, comes the disadvantage that these organic semiconductor thin films exist in kinetically trapped semicrystalline or polycrystalline states.[3] Recent studies have thus focused on elucidating how such structural heterogeneities impact device performance. In OTFTs with semicrystalline active layers, for example, the overall degree of crystallinity in the active layer has been positively correlated with an improvement in OTFT mobility.[4,5] In solution-processed OTFTs comprising polycrystalline active layers, nanoscale boundaries between crystalline domains have been shown to be bottlenecks for charge transport.[6,7] Because such heterogeneities have enormous impact on OTFT performance, it is critical to understand how structures over these relevant length scales in solution-processed organic semiconductor thin films affect charge transport. A firm understanding of these phenomena will generate design rules and guidelines for engineering materials and devices with improved performance.

Our study focuses on one such particular structure. Spherulites are frequently observed in polycrystalline solution-processed organic semiconductor thin films.[8−12] In spun-cast triethylsilylethynyl anthradithiophene (TES ADT; chemical structure in Scheme 1) films, for example, spherulitic growth can be induced by exposing the films to 1,2-dichlorethane solvent vapor.[9] During solvent-vapor annealing, TES ADT spherulites grow at a constant rate until they impinge, with average spherulite

* Address correspondence to lloo@princeton.edu.

Received for review July 31, 2012 and accepted September 30, 2012.

Published online September 30, 2012
10.1021/nn303446h

© 2012 American Chemical Society

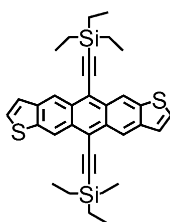

Scheme 1. Chemical structure of TES ADT.

diameters reaching over 3 mm.[13] These crystalline superstructures emanate from a single nucleation point and incorporate a distribution of orientations about the radial axis. Using grazing-incidence X-ray diffraction (GIXD), we found TES ADT to crystallize with its mean π-stacking direction aligned along the macroscopic radial axis of spherulites and a 40° spread in molecular orientation about the mean orientation.[13] To accommodate such a large spread in molecular orientations, TES ADT spherulites thus comprise many grains, each separated by low-angle grain boundaries.[14] Between neighboring spherulites, alternately, interspherulite boundaries (ISBs) exist, the widths of which are also expected to be on the nanoscale. Depending on the angle of impingement, these ISBs can be low and/or high angle in nature. Given the presence of intra- and interspherulite boundaries, the structure of spherulite-containing organic semiconductor thin films is complex. Yet, their individual contribution to macroscopic charge transport across polycrystalline films is not known. Exploiting a method to pattern spherulitic growth,[13] we have quantified the resistances across intraspherulite grain boundaries, as well as low- and high-angle ISBs. Intriguingly, we find charge transport across ISBs in solution-processed organic semiconductor thin films to be characteristically different from that across grain boundaries in thermally evaporated organic semiconductor thin films.

Previously, our investigation of solution-processed TES ADT thin films had indicated that ISBs in the active layers of OTFTs can significantly impact device mobility.[6] Specifically, by varying the spherulite size in the active layers of TES ADT OTFTs, we found device mobility to negatively correlate with the number of ISBs in the active channel.[6] While these results demonstrate that ISBs in general act as barriers to charge transport, the microscopic details of how low- and high-angle ISBs contribute to device resistance remains unclear. Such studies have in large part been hindered by difficulties in isolating ISBs having specific angles of molecular orientation mismatch. Borrowing from the terminology used in examining the structuring in organic small-molecule[15,16] and block copolymer[17,18] thin films, the angle of molecular orientation mismatch is defined by the vector normals of the two propagating fronts of neighboring grains.

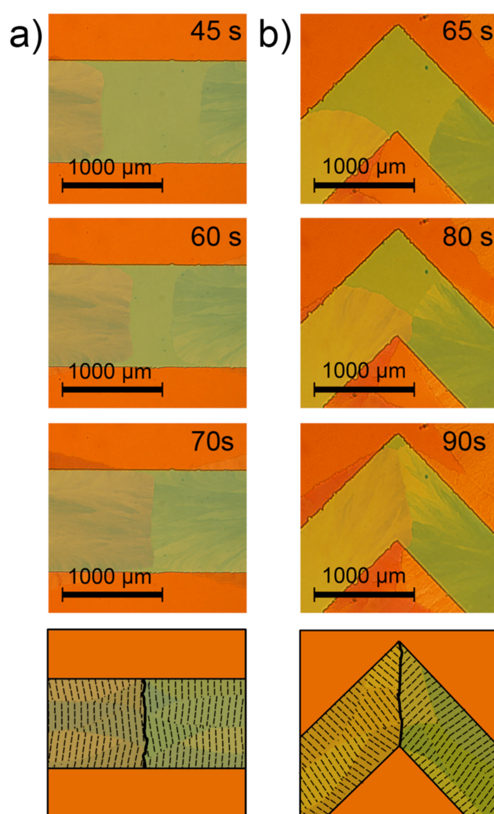

Figure 1. Time-lapsed images of crystallization in TES ADT thin films ultimately resulting in the formation of a (a) low-angle ISB having an angle of molecular orientation mismatch of 0 ± 20° and (b) high-angle ISB having an angle of molecular orientation mismatch of 90 ± 20°. Bottom images illustrate the molecular orientation of TES ADT molecules within the crystalline channels, with lines representing the conjugated π-planes of TES ADT. The black solid lines traversing the channel schematize the ISBs.

In the specific case of spherulites in which the crystallization fronts sample a broad distribution of molecular orientations, this angle of molecular orientation mismatch can vary along the lengths of ISBs. Isolating ISBs having specific angles of molecular orientation mismatch thus represents a yet more formidable challenge. Our ability to disrupt the radial growth of spherulites and guide TES ADT crystallization along arbitrary paths[13] has allowed us to engineer exclusively low- and exclusively high-angle ISBs and to quantify their resistivities and elucidate their contributions toward charge transport in TES ADT OTFTs.

RESULTS AND DISCUSSION

By patterning the underlying substrate to have regions of different surface energies, we can vary TES ADT crystallization rate by 3-fold during solvent-vapor annealing.[13] The ability to vary crystallization rates through prepatterning of substrates has thus allowed us to guide the crystallization of TES ADT in-plane along arbitrary paths.[13] Figure 1a shows the crystallization of TES ADT in which nucleation occurred at two separate points along a straight SiO_2 path surrounded

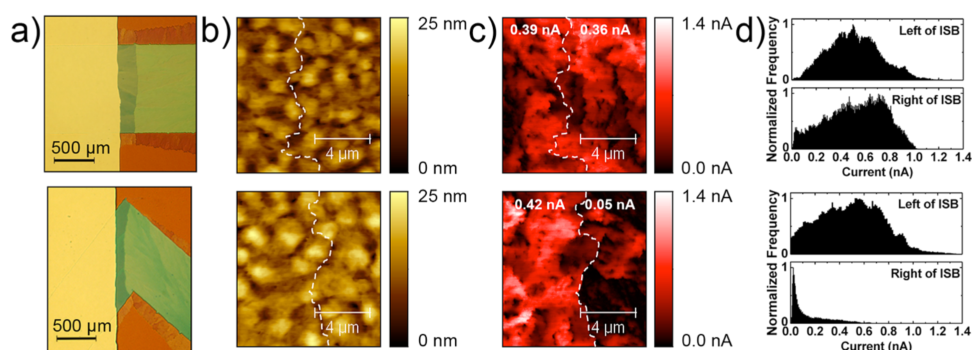

Figure 2. (a) Optical micrographs of TES ADT films comprising a low-angle ISB having an angle of molecular orientation mismatch of 0 ± 20° (top) and a high-angle ISB having an angle of molecular orientation mismatch of 90 ± 20° (bottom), with top-contact gold electrodes evaporated atop and to the left of the ISBs. (b) AFM height images collected in contact mode across the ISBs (indicated by the white dashed lines). (c) Corresponding current maps collected simultaneously with height images shown in (b) at an applied bias of +2 V. Average current levels of the regions before and after the ISBs are labeled for clarity. (d) Corresponding histograms that tabulate the frequencies of current levels of the regions before and after the ISBs. Frequencies are normalized by the maximum frequency observed for each region.

by pentafluorobenzenethiol (PFBT)-treated Au. Because the crystallization rate of TES ADT is almost three times higher on SiO_2 compared to that on PFBT-treated Au, at 24 ± 3 and 9 ± 3 μm/s, respectively, the crystallization fronts are preferentially guided along the SiO_2 path. When the crystallization fronts meet, a low-angle ISB is formed. Because a 20° spread in molecular orientation exists in either direction about the fast-growth axis at the propagation front,[13] the angle of molecular orientation mismatch is 0 ± 20°. When crystallization is instead directed along a SiO_2 path with a 90° corner, a high-angle ISB is formed, as shown in Figure 1b. In this case, the angle of molecular orientation mismatch is 90 ± 20°. It is important to note that because nucleation of spherulites is spatially random throughout the films, the meeting of two growth fronts at the 90° corner thus remains stochastic. We had to make several samples in order to obtain the desired high-angle ISB having an angle of molecular orientation mismatch of 90 ± 20°. The relative orientations of TES ADT illustrated in the bottom images of Figure 1, with black lines representing its π-plane, are based on our prior GIXD measurements.[13]

To visualize charge transport across single ISBs, we employed conductive AFM. Au electrodes were deposited *via* thermal evaporation on top of the TES ADT films to the left of the ISBs. A conductive AFM tip was used as the second electrode to collect current. Figure 2a shows optical micrographs of a sample with a low-angle ISB having an angle of molecular orientation mismatch of 0 ± 20° (top) and a sample with a high-angle ISB having an angle of molecular orientation mismatch of 90 ± 20° (bottom). Figure 2b shows contact-mode height images of the two films shown in Figure 2a near the ISBs (rms = 6 nm). The dotted lines indicate the location of the ISBs. Current maps were simultaneously collected over the same regions in the absence of a gate bias and at an applied bias of 2 V across the tip and gold electrode; these maps are shown in Figure 2c, with corresponding histograms accounting for the frequencies of currents in Figure 2d. For three low-angle ISBs having an angle of molecular orientation mismatch of 0 ± 20°, the average currents before and after the ISBs are 0.42 ± 0.02 and 0.38 ± 0.01 nA, respectively. The current drop across low-angle ISBs is small; this observation indicates that when the angle of molecular orientation mismatch between adjacent spherulites is small, the ISBs do not present significant hindrances to charge transport. On the other hand, the same experiment across high-angle ISBs having an angle of molecular orientation mismatch of 90 ± 20° affords an order of magnitude drop in current levels from 0.52 ± 0.1 to 0.06 ± 0.01 nA across the ISB. These results demonstrate that the angle of molecular orientation mismatch can significantly impact the ability for charges to travel across the ISBs, presumably—much akin to differences in low- and high-angle grain boundaries in polymer-based organic semiconductor thin films[19]—due to the extensive structural disorder at high-angle ISBs compared to those that may exist at low-angle ISBs.

To quantitatively measure the resistance of ISBs, we performed four-probe measurements during which contact resistance can be effectively eliminated. Using transmission electron microscopy (TEM) grids as shadow masks, we evaporated an array of Au electrodes *via* thermal evaporation on top of TES ADT thin films such that a single ISB having a prespecified angle of molecular orientation mismatch is located between the two inner electrodes of our four-probe setup and traverses the length of the electrodes. As a control experiment, we also evaporated four contact pads within a single spherulite to evaluate the intraspherulite resistivity of TES ADT. Figure 3a shows optical micrographs of the four-probe configuration on solvent-vapor-annealed TES ADT thin films with no ISB (but intraspherulite boundaries exist; left), a low-angle ISB having an angle of molecular orientation mismatch

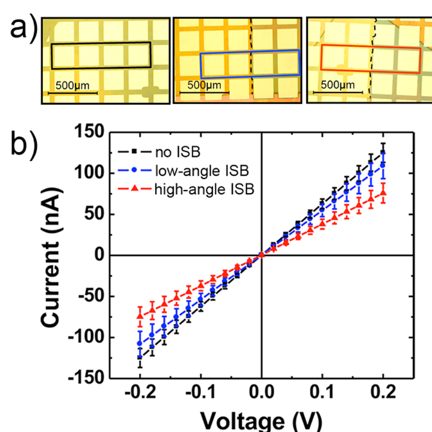

Figure 3. (a) Optical micrographs of TES ADT films with an array of gold pads evaporated on top. The gold pads were aligned on TES ADT films such that there is either no ISB (left), a single low-angle ISB having an angle of molecular orientation mismatch of 0 ± 20° (middle), or a single high-angle ISB having an angle of molecular orientation mismatch of 90 ± 20° (right) that traverses the entire channel of a four-probe geometry in which the gold pads act as electrodes. The colored rectangles highlight the set of electrodes used during measurements. The dashed lines indicate the position of the ISB. (b) *I*−*V* characteristics from four-probe measurements on the TES ADT films, color-coded to match the devices in (a). Four samples were tested for each of the three configurations. Error bars represent the spread of the *I*−*V* characteristics of the four samples.

of 0 ± 20° (middle), and a high-angle ISB having an angle of molecular orientation mismatch of 90 ± 20° (right) traversing the inner Au electrodes. Four-probe measurements were then collected in the absence of a gate bias using the four electrodes highlighted by the colored boxes in Figure 3a. Figure 3b shows the average current−voltage (*I*−*V*) characteristics of four devices of each configuration, with error bars representing the standard deviation of the measured current levels. The *I*−*V* characteristics are color-coded to match the device configurations in Figure 3a. As can be seen from the figure, the *I*−*V* characteristics of the devices with no ISBs and those with low-angle ISBs having an angle of molecular orientation mismatch of 0 ± 20° are comparable, with resistances of 1.6 ± 0.1 and 1.8 ± 0.1 MΩ, respectively. These results suggest that the resistivity across low-angle ISBs are comparable to resistivities measured within single spherulites. Because the radially symmetric nature of spherulitic growth mandates the presence of a distribution of molecular orientations along any given radial axis of the spherulite, single spherulites in fact comprise many individual grain boundaries. These intraspherulite boundaries are characterized by a low angle of molecular orientation mismatch,[20] rendering them structurally similar to low-angle ISBs. In contrast, devices with high-angle ISBs having an angle of molecular orientation mismatch of 90 ± 20° exhibit a resistance of 2.7 ± 0.3 MΩ. It thus appears that ISBs characterized by a high angle of molecular orientation mismatch pose larger barriers to charge transport compared to low-angle ISBs or low-angle intraspherulite boundaries. Supporting the work of Salleo and coworkers stating that high-angle boundaries present more significant barriers to charge transport compared to low-angle boundaries in polymeric semiconductor thin films,[19] our results indicate that ISBs in solution-processed organic semiconductor thin films are not all equivalent; the angle of molecular orientation mismatch at boundaries between crystalline domains can impact charge transport to varying extents, with the presence of high-angle ISBs more adversely affecting electrical characteristics.

To quantitatively compare our results with literature reports on grain boundaries in thermally evaporated organic semiconductor thin films,[21,22] we calculated resistivities from the measured resistances. To estimate the resistivity of ISBs in TES ADT thin films, we subtracted the resistance measured across films with no ISBs from those of films with a high-angle ISB having an angle of molecular orientation mismatch of 90 ± 20° and then scaled this difference by the length of the ISB and film thickness. We opted not to scale against the width of the ISB given the large uncertainty associated with its measurement. With this analysis, we found the resistivity of high-angle ISBs to be 22 MΩμm^2/(width of the ISB). For comparison, we estimated the resistivity across a low-angle grain boundary to be 450 MΩμm^2/(width of grain boundary) from a measured resistance of 25 GΩ in the absence of a gate bias across a single grain boundary having an angle of molecular orientation mismatch of 10° in thermally evaporated sexithiophene thin films.[22] We note that our comparison does not take into account the impact of the presence of accumulated charges at the organic semiconductor/dielectric interface on boundary resistance. TES ADT OTFTs display positive threshold voltages ranging from 5 to 26 V depending on processing conditions,[6,20] suggesting charge accumulation even in the absence of a gate bias. Such charge accumulation may in turn decrease the resistivity of the ISB.[22] On the other hand, sexithiophene OTFTs exhibit a threshold voltage of 0.9 V,[22] so a smaller degree of charge accumulation is present in the absence of gate bias compared to TES ADT OTFTs. However, even in the limit where the grain boundary resistivity in the sexithiophene sample achieves a minimum value of 90 MΩμm^2/(width of grain boundary) at an applied gate bias of −10 V, its resistivity is still four times larger than that of high-angle ISBs in TES ADT thin films measured at no applied gate bias. There thus appears to be distinct differences in charge transport across ISBs in solution-processed films and that across grain boundaries in thermally evaporated films, with our ISBs being substantially less resistive compared to grain boundaries in thermally evaporated thin films. Adding to this difference is the fact that the sexithiophene grain boundary in question is low-angle in nature;

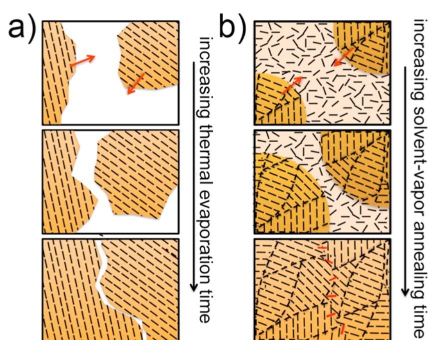

Figure 4. Illustration of how (a) grain boundaries in thermally evaporated thin films and (b) ISBs in solution-processed thin films form. Arrows indicate the direction of fast growth. Black lines represent the π-planes of the organic semiconductor. Red lines in the bottom right image indicate molecules bridging the ISB.

while the resistance of high-angle grain boundaries was not reported, it is presumably higher than that of low-angle grain boundaries. We note that the difference in chemical structures of sexithiophene and TES ADT may add to the discrepancy in the resistivities calculated, but we expect this contribution to be minor compared to the difference between the nature of the boundaries in thermally evaporated and solution-processed thin films. Given the vastly different deposition techniques, the widths of grain boundaries in thermally evaporated thin films and ISBs in solution-processed thin films and their extents of structural disorder must be different, and we believe it is such structural differences that are responsible for the large discrepancy in resistivities.

By examining the respective manners in which thermally evaporated and solution-processed organic semiconductor thin films are formed, we hope to shed light on the differences between grain boundaries and ISBs. Figure 4a schematizes film formation during thermal evaporation of organic semiconductors. In this case, molecules in the vapor phase nucleate on the substrate surface during deposition. Grain growth thus occurs simultaneously as the molecules are condensed on the substrate, progressively filling in the empty spaces on the substrate as neighboring grains grow toward each other. This process of grain growth during film formation leads to grain boundaries that may incorporate voids on the submicrometer length scale.[23] In fact, atomic force microscopy (AFM) conducted on thermally evaporated polycrystalline films of pentacene revealed crevices at these grain boundaries, extending almost the entire depth of the films.[22,24,25] In solution-processed organic semiconductor thin films, and in TES ADT thin films especially, the material comprising the final film is deposited all at once as a uniform layer and crystallization takes place upon solvent evaporation or on subsequent solvent-vapor annealing so there should be no microscopic voids or crevices at the ISBs where neighboring spherulites impinge. Consistent with this speculation are our failed attempts to image the ISBs of TES ADT, even by high-resolution AFM in topography mode (refer to Figure 2b). Instead, we had to use signals generated from transverse shear microscopy,[15] the magnitude of which depends on the relative orientation of the molecules, in conjunction with optical microscopy, to identify the location of ISBs. Grain boundaries in thermally evaporated organic semiconductor thin films, on the other hand, are easily captured by AFM operating in topography mode.[22,25] Figure 4b illustrates the growth of spherulites during solvent-vapor annealing of a film that had been deposited from solution. As shown in the figure, molecules that are present between the spherulitic growth fronts can be trapped as two neighboring spherulites impinge. Despite not being oriented in the same direction with respect to the fast growth direction of either of the impinging spherulites, these molecules (colored in red in the figure) can still bridge adjacent crystalline domains to transport charge across boundaries, decreasing the overall boundary resistance compared to grain boundaries in thermally evaporated thin films. In fact, the presence of polymer chains bridging grain boundaries in semiconducting polymer thin films has been reported to improve electrical connectivity between grains.[7] In a similar fashion, we believe TES ADT molecules that are trapped at ISBs may improve charge transport across these boundaries, resulting in an overall decrease in resistivity of ISBs in solution-processed thin films compared to grain boundaries in thermally evaporated thin films.

Finally, to correlate charge transport across microscopic ISBs with macroscopic OTFT mobilities in which the active layers comprise multiple ISBs, we examined the current−voltage ($I-V$) characteristics of OTFTs comprising varying numbers of ISBs in the active layers. We previously reported that TES ADT OTFT mobilities were positively correlated with the average spherulite size in the active layer.[6] In that study, we added between 0.5 and 7 mol % of fluorinated 5,11-bis-(triethylsilylethynyl)anthradithiophene, F-TES ADT, which acts as seeds to nucleate TES ADT crystallization, thereby varying TES ADT spherulite sizes from 3000 to 30 μm without perturbing the crystal structure or the electrical properties of TES ADT.[6,26] The number of ISBs in the active channel, calculated by dividing the channel length by the average spherulite diameter, correspondingly increased from 0.2 to 21 with increasing F-TES ADT, which correlated with an OTFT mobility decrease from 0.35 to 0.07 $cm^2/V \cdot s$. Here, we examine the consistency between these macroscopic measurements of charge transport through the active channels of OTFTs comprising multiple spherulites and ISBs and our measurements of charge transport across single ISBs by modeling spherulites and ISBs in the active channels of OTFTs as resistors in series. Specifically,

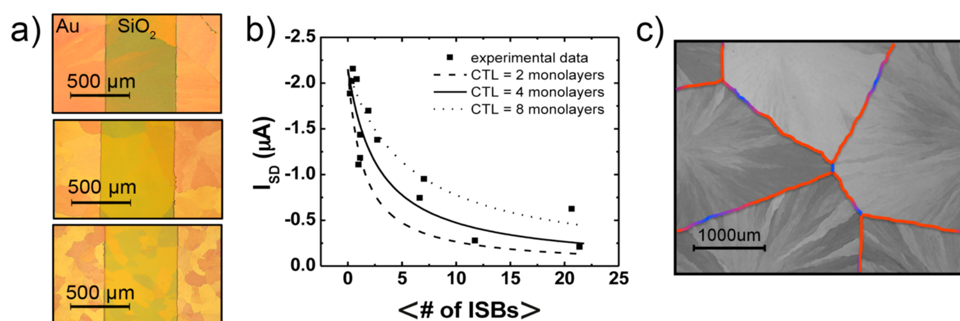

Figure 5. (a) Top view of the channel region of TES ADT transistors with varying spherulite size with Au and SiO_2 regions of the underlying substrate labeled. The top transistor has on average no ISBs traversing the length of the channel, the middle transistor has on average one ISB, and the bottom transistor has on average six ISBs across the channel. (b) Graph of the source−drain current measured at a source−drain voltage, V_{SD}, of −5 V and a gate voltage, V_G, of −10 V for transistors as a function of the average number of ISBs in the channel. The lines represent the calculated current using the resistivity of the high-angle ISB having an angle of molecular orientation mismatch of 90 ± 20° ISB extracted from four-probe measurements, assuming that the charge transport layer is 2 (dashed), 4 (solid), and 8 (dotted) monolayers thick. (c) Optical micrograph of a TES ADT thin film with ISBs highlighted. Blue indicates regions of the ISBs having a low angle of molecular orientation mismatch, while red indicates regions of the ISBs having a high angle of molecular orientation mismatch.

we extracted the output current from the linear regime of the OTFT output characteristics at a source−drain voltage and gate voltage of −5 and −10 V, respectively, and compared these values to the expected current levels calculated from Ohm's law, where the resistance is assumed to be a sum of the spherulite and ISB resistances. For these calculations, we assumed the resistance of ISBs to solely comprise that of the high-angle ISBs having an angle of molecular orientation mismatch of 90 ± 20°. By using the resistivity of high-angle ISBs measured at no applied gate bias for these calculations, we also assumed the resistivity of ISBs to be independent of gate voltage between 0 and −10 V. This assumption is in agreement with our observation that the relative current levels before and after ISBs, and thus resistivities of the ISBs, in conductive AFM measurements do not vary with increasing gate biases in this range. Figure 5a displays optical micrographs of the channel region of TES ADT OTFTs comprising 0 mol % (top), 0.75 mol % (middle), and 1.4 mol % (bottom) F-TES ADT relative to TES ADT, corresponding to 0, 1, and 6 ISBs in the active channel. To calculate the expected source−drain currents for TES ADT OTFTs comprising active layers with varying numbers of ISBs based on the resistivity we measured for isolated high-angle ISBs having a molecular orientation mismatch of 90 ± 20°, we assumed a simple resistors-in-series model in which the total resistance across the channel is

$$R_{total} = 2R_{contact} + (\#\text{ of spherulites}) \times R_{spherulite} + (\#\text{ of ISBs}) \times R_{ISB} \quad (1)$$

where R_{total} is the total resistance experienced by the transistor in the linear regime and can be extracted by normalizing the applied source−drain potential with the corresponding source−drain current; $R_{contact}$ is the contact resistance associated with injecting and extracting charges from the Au electrodes into and out of the active layer; $R_{spherulite}$ is the resistance of a spherulite, and R_{ISB} is the resistance across an ISB. For these calculations, we assumed that the ISBs are all high angle in nature, possessing a resistivity of 22 MΩμm^2/(width of ISB). Using the device with no ISBs in the channel region, we estimated the sum of the first two terms in eq 1 to be 1.5 MΩ. The source−drain current, I_{SD}, was calculated using Ohm's law $V = IR$ and was scaled by the thickness of the charge transport layer, t_{CTL}. Previously, the field-induced conductance of α-hexathienylene OTFTs was determined to be independent of film thickness beyond 5 nm.[27] Given that the molecules are organized in an edge-on orientation, this finding indicates that charge transport occurs primarily in the first few monolayers of α-hexathienylene thin films at the active layer−dielectric interface. By leaving t_{CTL} as a floating parameter during data fitting, we can thus estimate the thickness of the charge transport layer in TES ADT OTFTs. Figure 5b shows the measured currents as a function of the number of ISBs compared to the expected currents, with the fit having t_{CTL} = 6.7 nm, or 4 monolayers of TES ADT, represented by the solid black line in Figure 5b. To assess the sensitivity of the fit to variations in t_{CTL}, we also plotted the dependence of the source−drain current on the number of ISBs for t_{CTL} = 3.4 and 13.4 nm, equivalent to charge transport occurring in the first 2 and 8 monolayers of TES ADT at the active layer−dielectric interface, respectively. Despite the spread in the fit, this exercise indicates that, consistent with literature reports using other organic semiconductor systems,[27] charge transport in TES ADT OTFTs is limited to the first few monolayers at the dielectric surface. Since we only accounted for the presence of high-angle ISBs in our simple model, that our model sufficiently describes our transistor output currents also indicates that high-angle ISBs are the primary bottlenecks to charge transport in TES ADT. Figure 5c displays an optical micrograph of

a TES ADT thin film; regions of the ISBs where the angle of molecular orientation mismatch are low (<15°) are highlighted in blue, and regions of the ISB where the angle of molecular orientation mismatch are high (>15°) are highlighted in red. From the figure, it is apparent that ISBs are dominated by high angles of molecular orientation mismatch. That both low-angle ISBs are lower in resistivity and are present in substantially lower densities compared to their high-angle counterparts reduces their influence on the macroscopic transport of charge across polycrystalline channels in TES ADT OTFTs.

CONCLUSION

In light of the impact that boundaries have on charge transport through polycrystalline organic semiconductor thin films, understanding the nature of these boundaries and how they influence charge transport is critical to the field of organic electronics. Our findings suggest that organic semiconductors deposited from solution in which crystallization results in spherulite formation are characteristically different from those deposited *via* thermal evaporation. Specifically, spherulitic growth in solution-processed organic semiconductor thin films avoids the formation of large crevices at grain boundaries in the active layers that contribute to high resistivities. Furthermore, low-angle ISBs do not pose a significant barrier to charge transport compared to low-angle intraspherulite grain boundaries. Instead, charge transport is limited by the presence of high-angle ISBs. Our findings suggest that methods to eliminate the presence of high-angle ISBs, such as guiding crystallization along straight paths such that all ISBs are characterized by low angles of molecular orientation mismatch, may be promising to improving overall OTFT device performance.

EXPERIMENTAL METHODS

Film Formation. SiO_2/doped-Si wafers (300 nm) purchased from Process Specialties were rinsed sequentially with acetone, isopropyl alcohol, and deionized water and then dried with house nitrogen. Then, 35 nm Au pads were evaporated onto SiO_2/doped-Si substrates through shadow masks *via* electron-beam deposition. The substrates were then immersed in a 7.5 mM solution of PFBT in ethanol for 20 min immediately after removal of the substrates from the evaporation chamber. Sonication in clean ethanol for 2 min removes physisorbed compounds resulting in selective adsorption of PFBT in the regions covered by Au. The samples were dried with nitrogen prior to TES ADT deposition. TES ADT was synthesized according to previously published procedures.[28] To form thin films, TES ADT was first dissolved in toluene at a concentration of 2 wt %. The solutions were allowed to sit for <4−5 min prior to spin coating. Fresh solutions were made for each subsequent spin coating to avoid photobleaching of TES ADT while in solution. The solutions were spun cast onto the substrates at 1000 rpm for 60 s, resulting in a final film thickness of 100 nm. After spin coating, the substrates were immediately transferred to a hot plate and annealed at 90 °C for 2 min in order to remove residual toluene.

Solvent-Vapor Annealing. Exposure of the samples to 0.019 vol % DCE solvent vapor in N_2 to induce large-scale crystallization of TES ADT was carried out using a solvent-vapor annealing setup described elsewhere.[13] During solvent-vapor annealing, the films were observed under an optical microscope. Solvent-vapor annealing was carried out until two TES ADT crystallization fronts met along the SiO_2 paths.

Conductive AFM Measurements. Conductive AFM images were collected using a Veeco Dimension NanoMan AFM. The AFM was operated in contact mode using conductive Veeco AFM tips (model SCM-PIT) with spring constants between 1 and 5 N/m. Prior to measurements, top-contact gold electrodes were evaporated on top of the TES ADT thin films to the left of the ISBs. Gold was evaporated thermally to avoid damage to the underlying film.[29] A +2 V bias was applied across the electrode and the tip, and no gate bias was applied while the tip scanned along the surface of the film. Current flow from the electrode to the tip was simultaneously collected with height information of the film surface.

Four-Probe Measurements. Top-contact Au electrodes were defined by thermally evaporating 80 nm thick Au through a TEM grid onto TES ADT thin films. The electrodes were 204 μm and were equally spaced 50 μm apart. For samples with low- and high-angle ISBs, the inner two electrodes were aligned such that the ISBs traversed the entire length of the electrodes. Four-probe measurements were conducted using an Agilent 4145B semiconductor parameter analyzer by flowing current through the outer two electrodes and measuring the voltage drop across the inner two electrodes in the absence of a gate bias.

OTFT Measurements. To fabricate TES ADT OTFTs, 2 nm Ti/50 nm Au electrodes were first deposited onto 300 nm SiO_2/doped-Si substrates *via* electron-beam deposition. TES ADT solutions (2 wt %) in toluene with varying amounts of F-TES ADT were then spun cast onto substrates. The films were thermally annealed at 90 °C and then exposed to DCE solvent vapor until crystallization was complete. OTFTs were tested using an Agilent 4145B parameter analyzer. A detailed description of OTFT device fabrication and testing can be found elsewhere.[6]

Conflict of Interest: The authors declare no competing financial interest.

Acknowledgment. We acknowledge support from the NSF MRSEC program through the Princeton Center for Complex Materials (Grant DMR-0819860), which also provided access to the PRISM Imaging and Analysis Center. This research was also supported by the SOLAR Initiative at the NSF (DMR-1035217). S.S.L. was supported by a National Defense Science and Engineering Graduate fellowship.

REFERENCES AND NOTES

1. Dimitrakopolous, C. D.; Malenfant, P. R. L. Organic Thin Film Transistors for Large Area Electronics. *Adv. Mater.* **2002**, *14*, 99–117.
2. Sirringhaus, H.; Kawase, T.; Friend, R. H.; Shimoda, T.; Inbasekaran, M.; Wu, W.; Woo, E. P. High-Resolution Inkjet Printing of All-Polymer Transistor Circuits. *Science* **2000**, *290*, 2123–2126.
3. Lee, S. S.; Loo, Y.-L. Structural Complexities in the Active Layers of Organic Electronics. *Annu. Rev. Chem. Biomol. Eng.* **2010**, *1*, 59–78.
4. Kline, R. J.; McGehee, M. D.; Kadnikova, E. N.; Liu, J. S.; Frechet, J. M. J.; Toney, M. F. Dependence of Regioregular Poly(3-hexylthiophene) Film Morphology and Field-Effect Mobility on Molecular Weight. *Macromolecules* **2005**, *38*, 3312–3319.
5. Lim, J. A.; Lee, H. S.; Lee, W. H.; Cho, K. Control of the Morphology and Structural Development of Solution-Processed Functionalized Acenes for High-Performance Organic Transistors. *Adv. Funct. Mater.* **2009**, *19*, 1515–1525.

6. Lee, S. S.; Kim, C. S.; Gomez, E. D.; Purushothaman, B.; Toney, M. F.; Wang, C.; Hexemer, A.; Anthony, J. E.; Loo, Y.-L. Controlling Nucleation and Crystallization in Solution-Processed Organic Semiconductors for Thin-Film Transistors. *Adv. Mater.* **2009**, *21*, 3605–3609.
7. Jimison, L. H.; Toney, M. F.; McCulloch, I.; Heeney, M.; Salleo, A. Charge-Transport Anisotropy Due to Grain Boundaries in Directionally Crystallized Thin Films of Regioregular Poly(3-hexylthiophene). *Adv. Mater.* **2009**, *21*, 1568–1572.
8. Giri, G.; Verploegen, E.; Mannsfeld, S. C. B.; Atahan-Evrenk, S.; Kim, D. H.; Lee, S. Y.; Becerril, H. A.; Aspuru-Guzik, A.; Toney, M. F.; Bao, Z. Tuning Charge Transport in Solution-Sheared Organic Semiconductors Using Lattice Strain. *Nature* **2011**, *480*, 504–508.
9. Dickey, K. C.; Anthony, J. E.; Loo, Y.-L. Improving Organic Thin-Film Transistor performance through Solvent-Vapor Annealing of Solution-Processable Triethylsilylethynyl Anthradithiophene. *Adv. Mater.* **2006**, *18*, 1721–1726.
10. Li, Y.; Wu, Y.; Liu, P.; Prostran, Z.; Gardner, S.; Ong, B. S. Stable Solution-Processed High-Mobility Substituted Pentacene Semiconductors. *Chem. Mater.* **2007**, *19*, 418–423.
11. Gawrys, P.; Boudinet, D.; Zagorska, M.; Djurado, D.; Verilhac, J.-M.; Horowitz, G.; Pécaud, J.; Pouget, S.; Pron, A. Solution Processible Naphthalene and Perylene Bisimides: Synthesis, Electrochemical Characterization and Application to Organic Field Effect Transistors (OFETs) Fabrication. *Synth. Met.* **2009**, *159*, 1478–1485.
12. Lloyd, M. T.; Mayer, A. C.; Subramanian, S.; Mourey, D. A.; Herman, D. J.; Bapat, A. V.; Anthony, J. E.; Malliaras, G. G. Efficient Solution-Processed Photovoltaic Cells Based on an Anthradithiophene/Fullerene Blend. *J. Am. Chem. Soc.* **2007**, *129*, 9144–9149.
13. Lee, S. S.; Tang, S. T.; Smilgies, D.-M.; Woll, A. R.; Loth, M. A.; Mativetsky, J. M.; Anthony, J. E.; Loo, Y.-L. Guiding Crystallization around Bends and Sharp Corners. *Adv. Mater.* **2012**, *24*, 2692–2698.
14. Flewitt, P. E. J.; Wild, R. K. *Grain Boundaries: Their Microstructure and Chemistry*; Wiley: New York, 2001.
15. Kalihari, V.; Tadmor, E. B.; Haugstad, G.; Frisbie, C. D. Grain Orientation Mapping of Polycrystalline Organic Semiconductor Films by Transverse Shear Microscopy. *Adv. Mater.* **2008**, *20*, 4033–4039.
16. Kowarik, S.; Broch, K.; Hinderhofer, A.; Schwartzberg, A.; Ossó, J. O.; Kilcoyne, D.; Schreiber, F.; Leone, S. R. Crystal Grain Orientation in Organic Homo- and Heteroepitaxy of Pentacene and Perfluoropentacene Studied with X-ray Spectromicroscopy. *J. Phys. Chem. C* **2010**, *114*, 13061–13067.
17. Harrison, C.; Angelescu, D. E.; Trawick, M.; Zhengdong, C.; Huse, D. A.; Chaikin, P. M.; Vega, D. A.; Sebastian, J. M.; Register, R. A.; Adamson, D. H. Pattern Coarsening in a 2D Hexagonal System. *Europhys. Lett.* **2004**, *67*, 800–806.
18. Segalman, R. A.; Hexemer, A.; Hayward, R. C.; Kramer, E. J. Ordering and Melting of Block Copolymer Spherical Domains in 2 and 3 Dimensions. *Macromolecules* **2003**, *36*, 3272–3288.
19. Salleo, A.; Kline, R. J.; DeLongchamp, D. M.; Chabinyc, M. L. Microstructural Characterization and Charge Transport in Thin Films of Conjugated Polymers. *Adv. Mater.* **2010**, *22*, 3812–3838.
20. Lee, S. S.; Loth, M. A.; Anthony, J. E.; Loo, Y.-L. Orientation-Independent Charge Transport in Single Spherulites from Solution-Processed Organic Semiconductors. *J. Am. Chem. Soc.* **2012**, *134*, 5436–5439.
21. Chwang, A. B.; Frisbie, C. D. Temperature and Gate Voltage Dependent Transport across a Single Organic Semiconductor Grain Boundary. *J. Appl. Phys.* **2001**, *90*, 1342–1349.
22. Kelley, T. W.; Frisbie, C. D. Gate Voltage Dependent Resistance of a Single Organic Semiconductor Grain Boundary. *J. Phys. Chem. B* **2001**, *105*, 4538–4540.
23. Meyer Zu Heringdorf, F. J.; Reuter, M. C.; Tromp, R. M. Growth Dynamics of Pentacene Thin Films. *Nature* **2001**, *412*, 517–520.
24. Dimitrakopoulos, C. D.; Mascaro, D. J. Organic Thin-Film Transistors: A Review of Recent Advances. *IBM J. Res. Dev.* **2001**, *45*, 11–27.
25. Knipp, D.; Street, R. A.; Volkel, A.; Ho, J. Pentacene Thin Film Transistors on Inorganic Dielectrics: Morphology, Structural Properties, and Electronic Transport. *J. Appl. Phys.* **2003**, *93*, 347–355.
26. Lee, S. S.; Muralidharan, S.; Woll, A. R.; Loth, M. A.; Li, Z.; Anthony, J. E.; Haataja, M.; Loo, Y.-L. Understanding Heterogeneous Nucleation in Binary, Solution-Processed, Organic Semiconductor Thin Films. *Chem. Mater.* **2012**, *24*, 2920–2928.
27. Dodabalapur, A.; Torsi, L.; Katz, H. E. Organic Transistors: Two-Dimensional Transport and Improved Electrical Characteristics. *Science* **1995**, *268*, 270–271.
28. Payne, M. M.; Odom, S. A.; Parkin, S. R.; Anthony, J. E. Stable, Crystalline Acenedithiophenes with up to Seven Linearly Fused Rings. *Org. Lett.* **2004**, *6*, 3325–3328.
29. Dickey, K. C.; Smith, T. J.; Stevenson, K. J.; Subramanian, S.; Anthony, J. E.; Loo, Y.-L. Establishing Efficient Electrical Contact to the Weak Crystals of Triethylsilylethynyl Anthradithiophene. *Chem. Mater.* **2007**, *19*, 5210–5215.